

**GROUND STATE STRUCTURES OF SMALL
BORON AND BORON-CARBON CLUSTERS VIA
DENSITY FUNCTIONAL TIGHT BINDING AND
DENSITY FUNCTIONAL THEORY**

LIAN MING HUEI

UNIVERSITI SAINS MALAYSIA

2019

**GROUND STATE STRUCTURES OF SMALL
BORON AND BORON-CARBON CLUSTERS VIA
DENSITY FUNCTIONAL TIGHT BINDING AND
DENSITY FUNCTIONAL THEORY**

by

LIAN MING HUEI

**Thesis submitted in fulfillment of the requirements
for the degree of
Doctor of Philosophy**

March 2019

ACKNOWLEDGEMENT

The completion of my Ph. D. study is the result of contributions from various parties. Firstly, I would like to thank my family for financial and moral support. They were always concern for my well-being and the progress of my study. I am thankful to my supervisor, Assoc. Prof. Dr. Yoon Tiem Leong, who has always been providing technical support and guidance throughout my study. My mentor, Dr. Lim Thong Leng from Multimedia University, had also shared his advice on the parameterization process. Their supervision ensured smooth progress throughout my study. In addition, I am grateful to Prof. Lai San Kiong and Dr. Yen Tsung Wen, from National Central University of Taiwan, for organizing the student exchange program and sharing of knowledge on Modified Basin Hopping. The financial support from the School of Physics to attend the 9th Asian Consortium on Computational Materials Science held is acknowledged. My colleagues in theory lab had provided me with valuable technical advice on installation and maintenance of software and hardware. They are Koh Pin Wai, Lee Thong Yan, Robin Chang Yee Hui, Soon Yee Yeen, Ong Yee Pin and Goh Eng Seng. Lastly I would like to thank the staffs in Physics School in USM who had provided much support throughout my study.

TABLE OF CONTENT

| | |
|-----------------------------|-------|
| ACKNOWLEDGEMENT | ii |
| TABLE OF CONTENT | iii |
| LIST OF TABLES | vi |
| LIST OF FIGURES | vii |
| LIST OF ABBREVIATIONS | xii |
| LIST OF APPENDICES | xv |
| ABSTRAK | xvi |
| ABSTRACT | xviii |

CHAPTER 1 - INTRODUCTION

| | |
|--|----|
| 1.1 Boron Clusters, Carbon Clusters and Boron-Carbon Clusters | 1 |
| 1.2 Theoretical Approaches to the Search for the Ground State Structures | 3 |
| 1.3 Motivation..... | 8 |
| 1.4 Problem Statement..... | 11 |
| 1.5 Objectives of this Study..... | 11 |
| 1.6 Scope of Work | 11 |
| 1.7 Structure of this Thesis | 12 |

CHAPTER 2 - THEORY

| | |
|--|----|
| 2.1 Density Functional Theory (DFT) | 14 |
| 2.2 Self-Consistency Charge DFTB | 17 |
| 2.2.1 Band-Structure Energy | 19 |
| 2.2.2 Energy due to Charge Fluctuation | 20 |
| 2.2.3 Assumptions Made in SCC-DFTB | 21 |
| 2.3 Modified Basin Hopping | 22 |

CHAPTER 3 - COMPUTATIONAL METHODOLOGY

| | | |
|-------|---|----|
| 3.1 | Finding Atomic Orbitals and Electron Density | 28 |
| 3.1.1 | SCF Convergence | 30 |
| 3.1.2 | Optimal Damping Algorithm (ODA) | 31 |
| 3.1.3 | Direct Inversion of the Iterative Subspace (DIIS) | 31 |
| 3.1.4 | Combining ODA and DIIS in SCF Iteration | 33 |
| 3.2 | Calculation of Matrix Elements..... | 35 |
| 3.3 | The Hubbard U Parameter | 36 |
| 3.4 | Repulsive Energy Term | 36 |
| 3.4.1 | Parameterization of SK Files (original version) | 37 |
| 3.4.2 | Reparameterization of SK Files | 40 |
| 3.5 | Testing of SK Files | 57 |
| 3.6 | Method for Systematic Investigation the Boron and Mixed Boron-Carbon Clusters | 58 |
| 3.7 | Vibrational Frequency Analysis | 61 |

CHAPTER 4 - LOWEST ENERGY STRUCTURES OF CARBON, BORON AND MIXED BORON-CARBON CLUSTERS FROM THE LITERATURE

| | | |
|-----|--|----|
| 4.1 | Carbon Clusters, C_n | 64 |
| 4.2 | Chemical Bonding in Boron Clusters and Boron-Rich Mixed BC Clusters | 65 |
| 4.3 | Boron Clusters, B_n | 65 |
| 4.4 | Mixed Boron-Carbon Clusters..... | 69 |

CHAPTER 5 - RESULTS AND DISCUSSION

| | | |
|-------|--|----|
| 5.1 | Parameterization of SK files: First Attempt | 75 |
| 5.1.1 | Tuning the confinement radii for the C-C SK file | 76 |
| 5.1.2 | The Effect of Variation in r_w on the LESs of Carbon Clusters..... | 82 |

| | | |
|-------|---|-----|
| 5.1.3 | The Effect of Variation in r_{den} on the LESs of Carbon Clusters..... | 84 |
| 5.1.4 | Benchmarking the Boron SK File Generated against Known Boron Clusters from the Literature | 85 |
| 5.1.5 | A Systematic Investigation of the Boron Clusters..... | 89 |
| 5.1.6 | Testing of the Boron-Carbon SK files | 101 |
| 5.2 | Parameterization of SK files: Second Attempt..... | 103 |
| 5.2.1 | Reparameterization of the C-C SK file..... | 104 |
| 5.2.2 | Reparameterization of the B-B SK File | 105 |
| 5.2.3 | Reparameterization of the B-C and C-B SK Files | 109 |
| 5.2.4 | A Systematic Investigation of the Mixed Boron-Carbon Clusters | 118 |
| 5.3 | LES of B_{30} and B_{40} | 125 |
| 5.4 | Concluding Remarks on the Parameterization of the SK Files Process | 128 |

CHAPTER 6 - CONCLUSION

| | | |
|-----|---|-----|
| 6.1 | Summary..... | 130 |
| 6.2 | Original Numerical Insight on the Parameterization Process of B-B, B-C, C-B, and C-C SK Files | 131 |
| 6.3 | New Findings in the Boron and Mixed Boron-Carbon Clusters | 132 |
| 6.4 | Future Work..... | 134 |

| | |
|-------------------------|-----|
| REFERENCES | 136 |
|-------------------------|-----|

APPENDICES

LIST OF PUBLICATIONS

LIST OF TABLES

| | | Page |
|-----------|--|-------------|
| Table 3.1 | Column (a) shows R_{sig} where significant change in repulsive energy occurs when the confinement radii varies from 2-5 times the covalent radii of boron and carbon atoms. The confinement radii were applied to obtain the atomic orbitals of boron and carbon atoms. Column (b) shows the B-B and B-C bond length where change in the bonding nature occurs, denoted by R_{chg} (in Bohr), shown by DFT calculation. Column (c) shows the value of R_{max} for each compound. | 51 |
| Table 5.1 | The maximum errors in terms of bond length and bond angle of C_5 , C_7 , and C_9 when compared against the results listed in reference (Orden & Saykally, 1998)..... | 83 |
| Table 5.2 | The maximum errors in terms of bond length and bond angle of B_6 and B_{10} and also the point group of B_8 | 86 |
| Table 5.3 | Comparison of B_3 - B_{20} LESs produced by in this study with the LESs from the references (Alexandrova et al., 2006; Tai et al., 2010; Tai et al., 2012). Column (a) and (b) show the LESs produced by MBH/DFTB using borg-0-1 and the SK file created in this thesis. Column (c) shows the LESs produced by EMBH while column (d) shows LESs reported by (Alexandrova et al., 2006) (for B_3 and B_4), (Tai et al., 2010) (for B_5 - B_{13} excluding B_8) and (Tai et al., 2012) (for B_{14} - B_{20})..... | 90 |
| Table 5.4 | A summary of MBH/DFTB and EMBH results when compared against Refs. (Alexandrova et al., 2006; Boustani, 1997; Boustani et al., 2011; Kato & Yamashita, 1992; Kiran et al., 2005; Romanescu et al., 2012; Tai et al., 2010; Tai et al., 2012). | 95 |
| Table 5.5 | Vibrational frequencies calculated for the LESs of B_{11} , B_{16} and B_{17} . Columns (a) show the vibrational frequency (cm^{-1}) while columns (b) show the intensity (km mol^{-1}). | 96 |
| Table 5.6 | The maximum errors in terms of bond length and bond angle of C_5 , C_7 and C_9 when compared against the results listed in reference (Orden & Saykally, 1998)..... | 104 |
| Table 5.7 | A summary of MBH/DFTB and EMBH results when compared against Refs. (Chuchev & BelBruno, 2004; Feng & Zhai, 2017; Pei & Zeng, 2008; Shao et al., 2008; Sharipov et al., 2015). | 124 |

LIST OF FIGURES

| | Page |
|---|-------------|
| Figure 2.1 Flow chart of DFT calculation using Kohn-Sham method. Adopted from Ref. (Oliveira et al., 2009)..... | 19 |
| Figure 3.1 Process flow used in this study..... | 27 |
| Figure 3.2 SCF procedure which adopts both ODA and DIIS to accelerate convergence of SCF loop..... | 34 |
| Figure 3.3 Least square fit of repulsive energy calculated for C-C SK files by considering the total energy of ethane, ethene and ethyne molecules at different interatomic distance..... | 39 |
| Figure 3.4 BSpline fit for repulsive energy using the data calculated from least square fit..... | 40 |
| Figure 3.5 (a) The repulsive energy of B ₂ H ₂ plotted as a function of interatomic distance. (b) and (c) show the HOMO at B-B bond length of 5.2 and 5.4 Bohr, respectively..... | 44 |
| Figure 3.6 (a) The repulsive energy of CBH ₃ plotted as a function of interatomic distance. (b), (c), (d) and (e) show the HOMO at B-C bond length of 5.4, 5.6, 5.8 and 6.0 Bohr, respectively..... | 45 |
| Figure 3.7 (a) The repulsive energy of CBH plotted as a function of interatomic distance. (b), (c) and (d) show the HOMO at B-C bond length of 2.2, 2.4 and 2.8 Bohr, respectively. (e), (f), (g) and (h) show the HOMO-1 at B-C bond length of 2.6, 2.8, 3.2 and 3.8 Bohr, respectively..... | 47 |
| Figure 3.8 (a) The repulsive energy of ethyne plotted as a function of interatomic distance. (b) and (c) showed the HOMO-1 at C-C bond length of 4.8 and 5.0 Bohr, respectively..... | 49 |
| Figure 3.9 The repulsive energy of B ₂ H ₂ plotted as a function of interatomic distance (a) before and (b) after the R_{\max} is adjusted..... | 53 |
| Figure 3.10 The repulsive energy of CBH ₃ plotted as a function of interatomic distance (a) before and (b) after the R_{\max} is adjusted..... | 54 |
| Figure 3.11 The repulsive energy of CBH plotted as a function of interatomic distance (a) before and (b) after the R_{\max} is adjusted..... | 55 |
| Figure 3.12 The repulsive energy of ethyne plotted as a function of interatomic distance (a) before and (b) after the R_{\max} is adjusted..... | 56 |

| | | |
|------------|--|----|
| Figure 4.1 | LES and LLIs of carbon clusters (Orden & Saykally, 1998)..... | 64 |
| Figure 4.2 | LES of boron clusters identified by refs (Alexandrova et al., 2006) (B ₃ , B ₄), (Tai et al., 2010) (B ₅ -B ₁₃) and (Tai et al., 2012) (B ₁₄ -B ₂₀)..... | 67 |
| Figure 4.3 | LES of boron clusters identified by refs (Wang et al., 2016) (B ₃₀) and (Zhai et al., 2014) (B ₄₀)..... | 69 |
| Figure 4.4 | LES for BC mixed clusters reported by refs. (Feng & Zhai, 2017; Pei & Zeng, 2008; Sharipov et al., 2015). Silver balls represent boron atoms..... | 71 |
| Figure 5.1 | Overlap matrix element versus bond length (in units Bohr) based on the electron density from confined atom solutions, with when $r_{\text{at}} = r_{\text{den}} = 2r_{\text{cov}}$ are shown in the form of crosses. The results from reference (Porezag et al., 1995) are indicated with square dots..... | 77 |
| Figure 5.2 | Hamiltonian matrix element versus bond length (in units Bohr) based on the electron density from confined atom solutions, when $r_{\text{at}} = r_{\text{den}} = 2r_{\text{cov}}$ are shown in the form of crosses. The results from reference (Porezag et al., 1995) are indicated with square dots..... | 78 |
| Figure 5.3 | Hamiltonian matrix element versus bond length (in units Bohr) using the electron density from free atom solutions (crosses). The confinement radius is $r_{\text{at}} = 2r_{\text{cov}}$. The results from reference (Porezag et al., 1995) are indicated as square dots..... | 79 |
| Figure 5.4 | Hamiltonian matrix element versus bond length (in units Bohr) using the electron density from free atom solutions (crosses). The confinement radius is $r_{\text{at}} = 5r_{\text{cov}}$. The results from reference (Porezag et al., 1995) are indicated as square dots..... | 81 |
| Figure 5.5 | Overlap matrix element versus bond length (in units Bohr) using the electron density from free atom solutions (crosses). The confinement radius is $r_{\text{at}} = 5r_{\text{cov}}$. The results from reference (Porezag et al., 1995) are indicated as square dots..... | 82 |
| Figure 5.6 | Row (a), (b) and (c) show the LESs produced by SK file with $r_{\text{at}} = 2r_{\text{cov}}, 3r_{\text{cov}},$ and $6r_{\text{cov}}$ which were not linear structure..... | 83 |
| Figure 5.7 | LES produced using SK files generated with $r_{\text{den}} = 2r_{\text{cov}}$ [in row (a)] and $r_{\text{den}} = 5r_{\text{cov}}$ [in row (b)], respectively. These are all 3D structures..... | 85 |

| | | |
|-------------|---|-----|
| Figure 5.8 | Boron LESs produced by the SK file with $r_{at} = 2r_{cov}, 3r_{cov}, 3.2r_{cov}, 3.3r_{cov}, 3.5r_{cov}, 4r_{cov},$ and $4.5r_{cov}$ which have different point group as the LESs reported by refs. (Boustani et al., 2011; Alexandrova et al., 2006; Boustani, 1997; Kiran et al., 2005; Kato & Yamashita, 1992; Romanescu et al., 2012; Tai et al., 2010; Tai et al., 2012; Zhai et al., 2003). Front view and side view of the 2D structure for B_8 and B_{10} are provided so that readers can differentiate whether the LESs have planar or quasi-planar structure. | 87 |
| Figure 5.9 | Boron LESs produced by the SK file with $r_{den} = 2r_{cov}$ and $5r_{cov}$ while $r_{at} = 3.2r_{cov}$. For $r_{den} = 5r_{cov}$, B_{10} structures generated by MBH failed to converge by DFTB+ using the relevant SK file. | 89 |
| Figure 5.10 | Comparison of B_3 - B_{20} LESs generated in this study with that of (Alexandrova et al., 2006) (for B_3 and B_4), (Tai et al., 2010) (for B_5 - B_{13} excluding B_8) and (Tai et al., 2012) (for B_{14} - B_{20}). For B_{14} , B_{16} - B_{20} , both top view and side view are provided. The LESs generated using MBH/DFTB with the SK file from borg-0-1 set and the SK file created in this study are shown in row (a) and (b) respectively. The LESs generated using EMBH and those reported in refs. (Alexandrova et al., 2006; Tai et al., 2010; Tai et al., 2012) are shown in row (c) and (d) respectively. | 91 |
| Figure 5.11 | Comparison of (a) the vibrational spectrum of B_{11} computed in this study with (b) the vibrational spectrum reported by Romanescu et al. (2012). (Reprint from (Romanescu et al., 2012) with permission from AIP Publishing) | 98 |
| Figure 5.12 | Comparison of (a) the vibrational spectrum of B_{16} computed in this study with (b) the vibrational spectrum reported by Romanescu et al. (2012). (Reprint from (Romanescu et al., 2012) with permission from AIP Publishing) | 99 |
| Figure 5.13 | Comparison of (a) the vibrational spectrum of B_{17} computed in this study with (b) the vibrational spectrum reported by Romanescu et al. (2012). (Reprint from (Romanescu et al., 2012) with permission from AIP Publishing) | 100 |
| Figure 5.14 | LES produced when the confinement radii for B and C were varied from $2r_{cov}$ to $5r_{cov}$. Rows (a) to (d) show the LESs when the confinement radii for B and C are equal to each other and take the value of $2r_{cov}, 3r_{cov}, 4r_{cov},$ and $5r_{cov}$, respectively. Rows (e) to (g) show the LESs when the confinement radius for B was $2r_{cov}$ and the confinement radius for C was $3r_{cov}, 4r_{cov},$ and $5r_{cov}$, respectively. Rows (h) to (j) show the LESs when the confinement radius for B was $3r_{cov}$ and the confinement radius for C was $2r_{cov}, 4r_{cov},$ and $5r_{cov}$, respectively. Rows (k) to (m) show the LESs when the confinement radius for B was $4r_{cov}$ and the confinement radius | |

| | |
|--|-----|
| for C was $2r_{\text{cov}}$, $3r_{\text{cov}}$, and $5r_{\text{cov}}$, respectively. Rows (n) to (p) show the LESs when the confinement radius for B was $5r_{\text{cov}}$ and the confinement radius for C was $2r_{\text{cov}}$, $3r_{\text{cov}}$, and $4r_{\text{cov}}$, respectively..... | 101 |
| Figure 5.15 The non-linear LESs produced by SK file with $r_{\text{at}} = 2r_{\text{cov}}$ | 104 |
| Figure 5.16 LES produced when the r_{at} for B was $3r_{\text{cov}}$ (row (a)), $3.2r_{\text{cov}}$ (row (b)), $3.5r_{\text{cov}}$ (row (c)), $3.8r_{\text{cov}}$ (row (d)), $4r_{\text{cov}}$ (row (e)), and $5r_{\text{cov}}$ (row (f)), respectively. B_2H_2 and B_2H_4 were used as reference structures..... | 105 |
| Figure 5.17 Comparison of LESs generated by the reparameterized SK file with the inclusion of B_2H_2 as one of the reference systems. Rows (a) and (b) show the LESs obtained with the SK file before and after the inclusion of B_2H_2 . Row (c) shows the LESs obtained at the DFT level reported by previous publications (Alexandrova et al., 2006; Tai et al., 2010; Tai et al., 2012)..... | 107 |
| Figure 5.18 LES produced when $R_{\text{max}} = 3r_{\text{cov}}$ Bohr for CBH and r_{at} for B and C were varied. The colors of boron and carbon atoms are silver and black respectively. Rows (a) to (c) show the LESs when r_{at} for B was $3r_{\text{cov}}$ and r_{at} for C was $3r_{\text{cov}}$, $4r_{\text{cov}}$, and $5r_{\text{cov}}$, respectively. Rows (d) to (f) show the LESs when r_{at} for B was $4r_{\text{cov}}$ and r_{at} for C was $3r_{\text{cov}}$, $4r_{\text{cov}}$, and $5r_{\text{cov}}$, respectively. Rows (g) to (i) show the LESs when r_{at} for B was $4r_{\text{cov}}$ and r_{at} for C was $3r_{\text{cov}}$, $4r_{\text{cov}}$, and $5r_{\text{cov}}$, respectively. Rows (j) to (l) show the LESs when r_{at} for B was $5r_{\text{cov}}$ and r_{at} for C were $2r_{\text{cov}}$, $2.3r_{\text{cov}}$, and $2.5r_{\text{cov}}$, respectively. Rows (m) and (n) show the LESs when r_{at} for B was $6r_{\text{cov}}$ and r_{at} for C was $2r_{\text{cov}}$ and $2.5r_{\text{cov}}$ respectively. Row (o) shows the LESs when r_{at} for B and C were $7r_{\text{cov}}$ and $2r_{\text{cov}}$ respectively..... | 111 |
| Figure 5.19 LES produced when $R_{\text{max}} = 3.6r_{\text{cov}}$ Bohr for CBH and r_{at} for B and C were varied. The colors of boron and carbon atoms are silver and black respectively. Rows (a) to (c) show the LESs when r_{at} for B was $3r_{\text{cov}}$ and r_{at} for C was $3r_{\text{cov}}$, $4r_{\text{cov}}$, and $5r_{\text{cov}}$, respectively. Rows (d) to (f) show the LESs when r_{at} for B was $4r_{\text{cov}}$ and r_{at} for C was $3r_{\text{cov}}$, $4r_{\text{cov}}$ and $5r_{\text{cov}}$, respectively. Rows (g) to (i) show the LESs when r_{at} for B was $5r_{\text{cov}}$ and r_{at} for C was $3r_{\text{cov}}$, $4r_{\text{cov}}$, and $5r_{\text{cov}}$, respectively. Rows (j) and (k) show the LESs when r_{at} for B was $5r_{\text{cov}}$ and r_{at} for C were $2r_{\text{cov}}$ and $2.5r_{\text{cov}}$, respectively. Rows (l) and (m) show the LESs when r_{at} for B was $6r_{\text{cov}}$ and r_{at} for C was $2r_{\text{cov}}$ and $2.5r_{\text{cov}}$, respectively. Row (n) shows the LESs when r_{at} for B and C were $5.5r_{\text{cov}}$ and $2.5r_{\text{cov}}$, respectively..... | 114 |

| | | |
|-------------|--|-----|
| Figure 5.20 | The LESs generated for B_1C_2 , B_2C_1 , B_1C_5 , B_5C_1 , B_1C_9 and B_8C_2 . The colors of boron and carbon atoms are silver and black, respectively. Row (a) and (d) are the LESs generated using the SK file with $R_{\max}=3.0$ Bohr. Row (b) and (e) are the LESs generated using the SK file with $R_{\max}=3.6$ Bohr. Row (c) and (f) are the LESs reported in refs. (Chuchev & BelBruno, 2004; Feng & Zhai, 2017; Pei & Zeng, 2008; Sharipov et al., 2015). | 117 |
| Figure 5.21 | Comparison of LESs produced in this study with the LESs from refs. (Feng & Zhai, 2017; Pei & Zeng, 2008; Sharipov et al., 2015). Rows (a) and (b) show the LESs at DFTB and DFT level respectively. Row (c) shows the LESs reported by publications (Feng & Zhai, 2017; Pei & Zeng, 2008; Sharipov et al., 2015). | 119 |
| Figure 5.22 | Comparison of (a) the LES of B_{30} generated using MBH/DFTB with (b) the LES reported by ref. (Wang et al., 2016). The front view (left) and side view (right) of the LES generated using MBH/DFTB are provided. | 126 |
| Figure 5.23 | Comparison of (a) the LES of B_{40} generated using MBH/DFTB with (b) the LES reported by ref. (Zhai et al., 2016). The side view (left) and top view (right) of the LES generated using MBH/DFTB are provided. | 127 |

LIST OF ABBREVIATIONS

| | |
|----------------|--|
| 2D | 2-dimension |
| 2e2c | two-electron two-center |
| 2e3c | two-electron three-center |
| 3D | 3-dimension |
| 6-31+G(3df,2p) | Split-valence basis set arising from the group of John Pople with 6 primitive Gaussian functions (G) fitted for core atomic orbitals. This basis set has two basis functions for valence shells that have 3 and 1 primitive Gaussian functions respectively. “+” sign indicates diffuse basis functions are included. Polarization functions are provided with 3 sets of d functions and one set of f functions on heavy atoms and 2 sets of p functions on hydrogens. |
| AM1 | Austin Model 1 |
| AMRD | Angular move and random displacement |
| B | Boron |
| B3LYP | A hybrid exchange-correlation functional, stands for Becke, 3-parameter, Lee-Yang-Parr. (Riken, n.d.) |
| B97-2 | A hybrid exchange -correlation functional, published by Wilson, Bradley, and Tozer. (Wilson, Bradley, Tozer, 2001) |
| B-B | Boron-boron |
| BC | Boron-carbon |
| BH | Basin Hopping |
| C | Carbon |
| CCD | Coupled-cluster doubles |
| CCSD | Coupled-cluster singles and doubles |
| CCSD(T) | CCSD and perturbative triple |
| CISD | Configuration interaction singles and doubles |
| CK | Coalescence Kick method |

| | |
|----------|---|
| CNDO/2 | Complete Neglect of Differential Overlap |
| CPUs | Central processing units |
| DFT | Density Functional Theory |
| DFTB | Density Functional Tight Binding |
| DIIS | Direct inversion of the iterative subspace |
| EMBH | Extended version of MBH |
| GA | Genetic Algorithm |
| GEGA | Gradient embedded genetic algorithm |
| GSS | Ground state structure |
| HF | Hartree-Fock |
| KS | Kohn-Sham |
| LES | Lowest energy structure |
| LLI | Low-lying isomer |
| MBH | Modified Basin Hopping |
| MBH/DFT | MBH/DFT is the second stage calculation where MBH is the global minimum search algorithm and DFT is used as the energy calculator. |
| MBH/DFTB | MBH/DFTB is the first stage calculation where MBH is the global minimum search algorithm and DFTB is used as the energy calculator. |
| MC | Monte-Carlo |
| MD | Molecular Dynamics |
| MM | Molecular Mechanics |
| MP4SDQ | 4th order Møller-Plesset expansion that includes only single, double, and quadruple substitutions |
| MPn | <i>n</i> -th order Møller-Plesset expansion |

| | |
|----------|--|
| NDDO | Neglect of Differential Diatomic Overlap |
| ODA | Optimal damping algorithm |
| PBE | A generalized gradient approximation (GGA) for exchange and correlation, published by Perdew, Burke, and Ernzerhof (1996a) |
| PES | Potential energy surface |
| PM1 | Parameterization Method |
| PSO | Particle Swarm Optimization |
| QCISD | Quadratic configuration interaction singles and doubles |
| RHS | Right hand side |
| RM1 | Recife Model 1 |
| SCC-DFTB | Self-consistency charge DFTB |
| SCF | Self-consistent field |
| SK | Slater-Koster |
| STO-nG | Minimal basis set with n primitive Gaussian orbitals fitted to a single Slater-type orbital (STO) |
| TZVP | valence triple-zeta polarization |
| XC | Exchange-correlation |

LIST OF APPENDICES

- Appendix A.1 Input File to Generate Matrix Element for BC atom pair using Psi4
- Appendix A.2 Input File to Generate Total Energy for B₂H₂ using ORCA
- Appendix A.3 Input File to Obtain the Molecular Orbital of Ethyne When C-C Bond Length is 1.0 Bohr
- Appendix A.4 Input File to Optimize Cluster at DFTB Level
- Appendix A.5 Input File to Perform Geometry Optimization for B₁C₉ Using deMon2k
- Appendix A.6 Input File to Vibrational Frequency Analysis for B₁₁ Using deMon2k
- Appendix B SK Files
- Appendix B.1 B-B SK File before Reparameterization
- Appendix B.2 B-B SK File after Reparameterization
- Appendix B.3 C-C SK File after Reparameterization
- Appendix B.4 B-C SK File after Reparameterization
- Appendix B.5 C-B SK File after Reparameterization

**STRUKTUR KEADAAN ASAS KLUSTER KECIL BORON DAN BORON-
KARBON MELALUI TEORI FUNGSIAN KETUMPATAN PENGIKATAN
KETAT DAN TEORI FUNGSIAN KETUMPATAN**

ABSTRAK

Tujuan kajian ini adalah untuk mencari struktur keadaan asas (GSS, ground state structure) kluster kecil boron ($B_3 - B_{20}$) dan boron-karbon (BC, boron-carbon), B_xC_y ($3 \leq x + y \leq 10$). Versi tambahan Basin Hopping yang diubahsuai (EMBH, extended version of Modified Basin Hopping) telah digunakan untuk pencarian minima global. Kaedah pengiraan ini mempunyai dua tahap. Pada kedua-dua tahap, algoritma pencarian minima global, Basin Hopping yang diubahsuai (MBH, Modified Basin Hopping), telah digunakan untuk menghasilkan struktur-struktur rawak. Bagi tahap pertama, struktur-struktur rawak dioptimumkan secara tempatan oleh kaedah Teori Fungsian Ketumpatan Pengikatan Ketat (DFTB, Density Functional Tight Binding) manakala pada tahap kedua, struktur-struktur rawak dioptimumkan secara tempatan dengan menggunakan Teori Fungsian Ketumpatan (DFT, Density Functional Theory). Pengiraan DFTB memerlukan fail-fail Slater-Koster (SK) yang sesuai dalam persekitaran kluster. Oleh itu, fail-fail SK yang berkenaan telah dijanakan untuk meramal struktur keadaan asas untuk kluster boron dan BC. Kajian sistematik kluster boron telah dijalankan dengan menggunakan fail SK yang dihasilkan dalam tesis ini. 16 dari 18 LES berpadanan atau kelihatan serupa dengan LESs atau isomer berbaring rendah (LLIs, low-lying isomers) yang dilaporkan oleh penerbitan terdahulu. Dalam kajian sistematik kluster BC, 44 struktur telah dikaji. LESs untuk tiga kluster, iaitu, B_3C_6 , B_3C_7 , dan B_9C_1 , yang belum dilaporkan dalam karya-karya lain, telah dikaji. 4 daripada 41 struktur yang

dikaji tidak berpadanan atau kelihatan serupa dengan LESs atau LLIs yang dilaporkan oleh penerbitan terdahulu. Kluster BC baru B_9C_1 yang kaya dengan boron diramalkan mempunyai dua atom boron pusat pada peringkat DFT, struktur ini berkelihatan serupa dengan LES B_{10} yang mempunyai struktur C_{2h} . Ramalan ini selaras dengan pemerhatian yang dibuat oleh Pei dan Zeng (2008) dimana kluster BC yang kaya dengan boron mempunyai yang serupa dengan LES dan LLIs kluster boron tulen. Bagi B_3C_6 dan B_3C_7 yang kaya dengan karbon, LESs yang dihasilkan mempunyai struktur planar tanpa atom boron pusat yang membentuk ikatan multi-pusat dengan atom sekitar. Kajian sebelum ini melaporkan bahawa LESs untuk kluster-kluster BC yang mempunyai 9 dan 10 atom dan kaya dengan karbon mempunyai struktur planar tanpa ikatan multi-pusat apabila jumlah atom boron dalam kluster ini adalah 1, 2 dan 4. Oleh itu, ramalan bagi B_3C_6 and B_3C_7 yang tidak mempunyai boron pusat adalah munasabah. Secara keseluruhan, penggunaan DFTB pada tahap pertama mengurangkan masa yang digunakan untuk pencarian minima global dan ramalan LESs boron dan BC kluster yang dibuat oleh EMBH adalah memuaskan.

GROUND STATE STRUCTURES OF SMALL BORON AND BORON-CARBON CLUSTERS VIA DENSITY FUNCTIONAL TIGHT BINDING AND DENSITY FUNCTIONAL THEORY

ABSTRACT

The objective of this study is to search for the ground state structure (GSS) of boron clusters ($B_3 - B_{20}$) and boron-carbon (BC) clusters, B_xC_y ($3 \leq x + y \leq 10$). The extended version of Modified Basin Hopping (EMBH) is used for the global minimum search. This is a two-stage calculation. In both stages, the global-minimization search algorithm, Modified Basin Hopping (MBH), is used to generate random structures. In the first stage, the random structures are locally optimized using Density Functional Tight Binding (DFTB) while in the second stage, the random structures are locally optimized using Density Functional Theory (DFT). The DFTB calculation requires Slater-Koster (SK) files that are conducive in a cluster environment. Hence, the relevant SK files are developed to predict the GSS for boron and boron-carbon clusters. A systematic study of boron clusters obtained using the SK files generated in this thesis has been carried out. 16 out of 18 LESs matched or mimicked with the LESs or LLIs reported by previous publications. In the systematic study of the BC clusters, a total of 44 structures have been studied. The LESs for three clusters, namely, B_3C_6 , B_3C_7 , and B_9C_1 , which have not been reported elsewhere, are studied. 4 out of 41 structures studied do not match or mimic the LESs or LLIs reported by previous publications. The new BC clusters, B_9C_1 , which is boron-rich, was predicted to have two middle boron atoms at DFT level, which mimics the LES for B_{10} which has C_{2h} structure. This is consistent with the observation made by Pei and Zeng (2008) where boron-rich mixed BC clusters have

structures similar to the LESs and LLIs of pure boron clusters. In carbon-rich B_3C_6 and B_3C_7 , the LESs generated have planar structures with no central boron atom forming multicenter bond with peripheral atoms. For carbon-rich mixed BC clusters of 9 and 10 atoms, planar structures LESs are reported by previous studies and multicenter bond is not formed for when the amount of boron atoms in these clusters are 1, 2 and 4. Hence predicting B_3C_6 and B_3C_7 with no central boron atom is reasonable. Overall, the use of DFTB in the first-stage calculation has reduced the time needed for the global minimum search and EMBH produces reasonable prediction for the LES of boron and BC clusters.

CHAPTER 1 - INTRODUCTION

A cluster is a group of atoms with size between a molecule and a bulk solid (Yang & Huang, 2017). These atoms can be held by metallic, covalent, ionic, hydrogen-bonded or Van der Waals (Doye, 1997). What distinguishes a cluster from a molecule? Firstly, the types of bond that can exist in a cluster can help to distinguish a cluster from a molecule. The intra-molecular force of attraction in a molecule is mainly covalent bond while atoms in a cluster can be bonded by metallic, covalent, ionic, hydrogen bonded or Van der Waals forces. Secondly, molecules are stable under ambient condition while clusters are not stable towards aggregation (Castleman & Jena, 2006). The cluster, which is discussed here, differs from the word “cluster” which was originally coined by F. A. Cotton in the early 1960s (Yang & Huang, 2017). Cotton introduced the term “metal atom cluster compounds” which referred to a group of metal atoms that held mainly by a metal-metal bond (Fedorov, 2015) while the cluster discussed here can be held by other types of bond. Clusters are of great scientific interest because of the evolution of properties with size (Jortner, 1992). Research conducted to study the properties of clusters has increased the understanding of the problems that exist in many areas of science.

1.1 Boron Clusters, Carbon Clusters and Boron-Carbon Clusters

Boron, carbon and boron-carbon clusters have been studied extensively due to their interesting properties and potential application. Georgakilas et al. (2015) classified the carbon nanoallotropes (fullerenes, carbon nanotubes, graphene and carbon dots) and described the properties according to their structures. Carbon dots show upconversion photoluminescence when they are excited using light of wavelength more than 600 nm. This property makes carbon dots potentially useful as

photocatalysis. Nanodiamonds are chemically stable, biocompatible and resistant to corrosion. Hence they can be potential solid carriers of drug and biomolecules. Carbon nanotubes can sustain extreme strain without indication of plasticity. They can be useful if this property can be translated into macroscopic scale to enhance the mechanical properties of polymers and carbon structures (Georgakilas et al., 2015). Researches have been conducted to investigate the structure of carbon clusters. Small carbon clusters ($C_3 - C_{20}$) are predicted in theoretical studies to have either linear or monocyclic structures. However linear structures were mostly observed up to C_{15} in the majority of experimental studies (Orden & Saykally, 1998).

Despite having poor conductivity, the boron-based material has a low density, a high melting point and hardness (Boustani, 1997). These mechanical characteristics have witnessed many applications, including the boron neutron capture therapy (Chakrabarti & Hosmane, 2012) appearing as magnetic nanocomposite materials, in industrial sectors where boron nitride are used as lubricant (AZoM Materials, 2009), in high-energy-density fuels due to its light weight (Demirbas, 2005; Ray et al., 1992). Bioorganic boron clusters have been used to design drugs and hence the study on the properties of boron-based cluster is of high interest in research community (Leśnikowski, 2016). Theoretical studies show that small boron clusters B_n of size $n < 19$ have planar structures. Experimental efforts are mostly conducted to study the structure of cations and anions of boron clusters but not on neutral boron clusters. These experimental results showed that B_{39}^- and B_{40}^- have 3D cage-like structure while B_{29}^- and B_{36}^- have quasiplanar structure with a hole at the center of the clusters (Li et al., 2016; Chen et al., 2015; Zhai et al., 2014; Piazza, 2014).

Boron-carbon (BC) compounds have been well known for their thermal stability, low density but high hardness and the ability to absorb neutrons (Everitt, Doggett, n.d.; Nam, et al. 2015; Pender & Sneddon, 2000). Boron carbide (B_4C_1) is often used as armor and abrasive due to its hardness (ESK Ceramic GmbH & Co. KG., 2014), coating due to its high heat and chemical resistance (Nevada Thermal Spray Technologies, n.d.) and fuel component of solid rocket propellant compositions (Jerome, 1958). Carborane, which composes of boron, carbon and hydrogen atoms, is used in the production of heat-resistant polymers (Williams, 1972) and carborane acid (Olah et al., 2009).

In the theoretical front, many investigations have been carried out to search for the lowest energy structure (LES) of mixed BC clusters using ab initio methods (Sharipov et al., 2015; Chuchev & BelBruno, 2004; Shao et al., 2008; Pei & Zeng, 2008; Feng & Zhai, 2017; Shao et al., 2010; Wang et al., 2013; He et al., 2011; Liu et al., 2008; Wang et al., 2007; Liu et al., 2007; Park, 2005). Chuchev and BelBruno compared the energy for carbon-rich BC clusters, i.e. BC_y and B_2C_y , and found that the linear structure and cyclic structure are almost isoenergetic when $y = 5$. However, when $y = 6 - 10$, the structures tend to be cyclic instead of linear (Chuchev & BelBruno, 2004). Pei and Zeng studied boron-rich BC clusters and observed that neutral boron-rich clusters have structures similar to the pure boron clusters (Pei & Zeng, 2008). In general, studies showed that the mixed BC nanoclusters are found to display linear, planar or quasi-planar structures.

1.2 Theoretical Approaches to the Search for the Ground State Structures

The physical properties of nanoclusters are determined by their ground state structure (GSS), defined as the structure with a configuration that is theoretically lowest in

total energy. Hence, identifying the GSS is the preliminary step for studying the physical properties of nanocluster theoretically. Locating the GSS involves a sequence of procedure of optimizing a collection of initial structures, calculating and comparing the energies of the optimized structures. Computationally speaking, this procedure is a global minimization search. The resultant structure appearing at the end of an attempted global minimization search with the lowest energy is known as the lowest energy structure (LES). In practice, the LES is taken to effectively represent the sought-after GSS, despite the former could be algorithm and procedure-dependence, while the latter is theoretically unique. Given a fixed composition of nanoclusters, different global minimization searches for the desired LES may end up with varying outcomes. The LES computationally obtained at the end of an unbiased global minimum search calculation is not unique, and strongly depending on two factors, namely, the efficiency and suitability of the global minimum search algorithm deployed (e.g., basin-hopping, genetic algorithm, particle swarm optimization, etc.) in the search strategy, and the level of theory used for calculating the total energy. The latter is referred to as the “energy calculator”, or just “calculator”. In the initialization stage of a global search, a pool of random initial structures is first created. A chosen energy calculator then performs local optimization on these input structures using a local optimization algorithm incorporated within it. The total energy of the locally optimized structure is evaluated by the energy calculator.

An energy calculator used in a search algorithm is operating based on a particular theory for calculating the total energy of an input configuration of the atoms in a cluster. Currently, many energy calculators are available with different level of theories. Largely, they can be grouped into three categories according to

increasing level of underlying robustness: (i) empirical, (ii) semi-empirical, and (iii) first-principles theories. In this thesis, the first-principles calculator will be exclusively referred to as that based on density-functional theory (DFT). DFT calculator consumes the largest computational resources and time. An example of a semiempirical calculator is density-functional tight-binding (DFTB), which is the major subject of this thesis. A typical example of an empirical calculator is molecular dynamics (MD), in which the dynamics among the atoms within a cluster is completely determined by some functional forms of empirical potentials. The accuracy, time and resource consumption to perform a calculation in DFTB lie in between that of empirical potentials and DFT.

For illustration purpose, consider two disparately different energy calculators, an empirical calculator based on molecular dynamics, a classical theory which must make use of an empirically derived potential (or so-called forcefield) and a first-principles calculator based on DFT. These two types of calculator belong to very disparate underlying theories. The former is empirically classical, while the latter is fully quantum mechanical and capable of capturing non-local electronic contributions in the formation of a stable cluster structure. In general, the landscape of the potential energy surface (PES) defined by the empirical calculator is different from that of a DFT energy calculator. Hence, the LES found in the PES of an empirical calculator may not be the same as that found in the PES of a DFT calculator. Theoretically, it is hard to quantify the comparison between two PES landscapes of different theoretical level, and this can only be discussed qualitatively and not without ambiguity. Having said that, it is consensual to assume that the “true” LES of a cluster should be that living in the PES of the DFT, which is the most fundamental framework for describing atomic interactions at the quantum

mechanical level. Theories such as empirical molecular dynamics and DFTB (or other contrived/derived models) are less “superior” comparatively, and the geometric configuration of the LES obtained at this level may or may not be similar to that at the DFT level. In terms of theoretical robustness to describe the interactions among the atoms in the clusters, DFT is considered the most superior and sits at the top of the theoretical hierarchy. DFTB being semi-empirical but still quantum mechanical (at least partly) sits at a level lower than DFT. The forcefields in the MD description of atomic interactions, being empirical in nature, are considered lowest in the theoretical hierarchy, although this may not necessarily mean its predictive power is always poor or unreliable, just that the formulation of MD forcefields, due to its empirical nature, does not explicitly capture the electronic contributions (which is quantum mechanical in nature) to describe the atomic interactions.

A global search strategy that involves an empirical energy calculator needs much lesser computational resource to locate the LES in the PES of the relevant empirical potential. However, such a LES so located does not have electronic contribution taken into account during the searching process. This may possibly lead to an inaccurate prediction of the GSS when compared to the prediction made at the DFT level, which is a fully quantum mechanical theory. In comparison to MD, DFTB is conceptually closer to DFT in the sense that DFTB, despite being semi-empirical, takes into account of electronic (quantum mechanical) effects in its parameterization (in terms of the SK files). Hence, one envisages, at least conceptually, the DFTB PES to have a closer fidelity to the DFT PES than MD does. The envisaged closer resemblance between the DFT and DFTB PES provides a possible intermediary path to computationally access the full PES of the DFT at a cheaper cost. By this way, the LES obtained at the end of a global minimum search

in the DFTB level could serve as an effective approximation to the ‘true’ LES at the DFT level. This is the underlying conjecture assumed by this thesis when designing the search strategy for locating the LES of the BC clusters.

In the research front for studying the ground state structures of clusters, some researchers identify the GSS with a search strategy that is categorized as ‘biased’ (in contrast to an ‘unbiased search’ which is adopted in this thesis). In a biased search, a pool of known or predefined structures (perhaps from some earlier reported results or preliminary studies or available data set) is assumed as initial configurations, from which the subsequent search for the GSS are initialized. One possible problem with this method is that certain seed configurations, which may be essential but are not known *a priori*, may have been excluded from the pool. In contrast, in the unbiased method, random configurations are generated *unbiasedly* (without any predefined structures as in the case of the biased search) as the initial seed configurations for the subsequent global minimization search. In this way, an unbiased search avoids the dependence on the knowledge of the pool of predefined structures. This is particularly convenient if no such pool of predefined structures is known. It also, to a certain extent, alleviates the possible consequences for missing out those essential but *a priori* unknown seed structures, a problem that could inflict the search for a true GSS. Examples of the unbiased global optimization search for the GSS of clusters are Genetic Algorithm (GA) (Zeiri, 1995), Basin Hopping (BH) (Wales & Doye, 1997), Particle Swarm Optimization (PSO) (Eberhart & Kennedy, 1995), to name a few.

In practice, at the end of an unbiased search for the GSS of a given cluster with fixed composition, one may obtain varying results, depending on (i) which energy calculator (i.e., which level of theory) is used, and (ii) which global

minimization algorithm is adopted (plus the details of the parameters used during the implementation of the search process). It turns out that the search strategy to locate the GSS of a cluster can be vastly diversified. It is not the intention of this thesis to perform a summarization or full review of the available methodologies. The endeavor to locate the true GSS to an extent is not entirely free of absolute ambiguity. The GSS is a structure not known a priori, and the LES obtained at the end of a computational procedure is dependent on wall-time spent, hardware resources available, technical details of the search strategy, and human patience. At one stage a certain configuration of atoms taken as the GSS could be replaced by another with a lower energy if discovered later via a different computational route. The true GSS obtained in this thesis, and indeed in all other reported findings, only represent the best-effort results at best, until they are supplanted by other even lower ones.

1.3 Motivation

As mentioned in the previous subsection, DFT is an expensive atomistic calculation. Identification of the ‘true’ GSS of a cluster, i.e., the GSS in the DFT PES is a daunting task. In performing self-consistent field (SCF) calculation, the evaluation of electron-electron repulsion and exchange-correlation energy in DFT is needed. On the other hand, semi-empirical quantum chemistry methods simplify the process of evaluating these terms. For example, Complete Neglect of Differential Overlap (CNDO/2) neglects many electron-electron repulsion terms and approximates some of the electron-electron repulsion terms (The Sherrill Group, n.d.). DFTB, which is also a semi-empirical method, stores the Hamiltonian term in the form of Slater-Koster (SK) file. This prevents integral evaluation during the SCF calculation. Molecular mechanics (MM), being an empirical method, calculates the total energy

as a function of interatomic distance, bond angle, torsional angle, etc. whereby the coefficient in these functions had been fitted using experimental data or theoretical calculation (Young, n.d.). Hence, in MM, there is no need to find the molecular orbital through SCF calculation. Comparing semi-empirical and empirical methods, DFT is more time consuming and resource consuming. One can envisage performing a global minimization in the DFT PES using a DFT calculator, but this sort of 'direct DFT global minimization' search strategy can be impractical due to its tremendously demanding computational cost. One of the motivations of this thesis is to provide a viable computational strategy for identifying the GSS of boron and BC clusters at the DFT level via a two-stage calculation procedure involving a semi-empirical method in the first stage while DFT in the second. Austin Model 1 (AM1) (Dewar et al., 1985), Parameterization Method (PM1) (Stewart, 1989), and Recife Model 1 (RM1) (Rocha et al., 2006) are the semi-empirical methods developed based on Neglect of Differential Diatomic Overlap (NDDO) integral approximation. They have many empirical parameters fitted to a set of molecular properties. This may limit the application of such methods (Oliveira et al., 2009). On the other hand, DFTB does not have requires large amount parameters fitted to experimental or theoretical data. As less empirical parameters are used in DFTB, the parameterization process is less complicated. DFTB has also been applied to calculate various properties such as the magnetic properties of iron clusters (Kohler et al., 2005), vibrational spectra of large molecules (Witek et al., 2004), geometries of carbon clusters (Yen & Lai, 2015) and many others, provided the suitable SK file is available. Due to these advantages offered by DFTB, DFTB will be used in the first stage during the search of the GSS of boron and BC clusters.

Another related motivation is to independently generate a set of SK files for B-B, B-C, C-B, and C-C interactions that aim to work in a cluster environment. DFTB is an approximation to DFT. DFTB per se can in principle be an accurate quantum mechanical calculation method at par with the DFT, provided that the relevant SK files are available and have been appropriately parameterized. The DFTB website (“The DFTB website”, 2017) provides free SK files that are widely used by the DFTB community. The parameterization process of DFTB involves fine-tuning a number of free parameters (Elstner & Seifert, 2014; Porezag et al., 1995). The SK files which can reproduce the results of some pre-selected systems are considered to provide a good description of the interaction for the atom pair of interest, at least in these systems. However, the free parameters which are found to be optimal for certain systems (molecular systems or bulk systems) may or may not work for the others (for example, cluster system). In other words, SK files parameterized for an element in the solid-state phase may not accurately describe the interaction between the same element in a cluster environment. This problem is well-known in the DFTB research community, and it is known as the transferability limit (Elstner & Seifert, 2014). As an example, consider the boron-boron (B-B) SK file in the borg-0-1 set (Grundkotter et al., 2012). This set of SK files had been tested for molecular and periodic systems. Yen et al. (Yen, 2014) used the same borg-0-1 set in their attempt to search for the LES for B_{20} and found that this parameter set produced unreasonably high energy in the double ring structure. As such, the issue of transferability must be taken into proper account when a set of SK files are adopted in a calculation (Elstner et al., 2000). This thesis fills up the research gap by providing researchers working with BC clusters the SK files that are specifically

generated to work in a cluster environment. Another motivation of the thesis is to search for novel, never-been-discovered BC structures.

1.4 Problem Statement

Identification the GSS of a cluster with a given composition in the DFT potential energy surface (PES) using an unbiased approach is demanding in terms of computational cost.

1.5 Objectives of this Study

1. To obtain the SK files for boron, carbon and boron-carbon interactions in cluster environment so that they can be used to study the GSS of pure boron, pure carbon and BC clusters.
2. To obtain the lowest energy structures of boron clusters, B_3 - B_{20} at DFTB and DFT level.
3. To obtain the lowest energy structures of BC clusters, B_xC_y where $1 \leq x, y \leq 9$, $3 \leq x + y \leq 10$, at DFTB and DFT level.

1.6 Scope of Work

The study on GSS of boron and BC clusters and lack of proper SK file for cluster environment has led to the development of B-B, C-C, and B-C SK files. This thesis does not assess the transferability limit of SK file to the non-cluster environment. It is stressed that these SK files are specifically tuned and derived with the specific aim to search for the GSS of boron and BC clusters. These parameters give a good description of the interaction between the atom pair of interest when the SK files are used for finding the GSS of a cluster in a cluster environment. However, the values

of these parameters may not be optimal in other scenarios. This has been mentioned in subsection 1.3. The obtained SK files are not been tested for calculation of the electronic and thermal properties of boron and BC clusters as the references systems used to parameterize the SK files are not meant for such purposes. In other words, this thesis does not stress-test the transferability limit of the SK by applying the SK files to calculate the electronic structures of the clusters using DFTB.

The self-consistent charge DFTB (SCC-DFTB) is used to conduct this study. SCC-DFTB takes into account the change in total energy up to second order of charge fluctuation. This theory breaks down in charged systems where the charges are localized (Reimers, 2011). The Hubbard U parameter, which is a constant parameter in SCC-DFTB, depends on the atom size. The atom size, in turn, depends on the charge state of the atom. For charged system with localized charges, the size of atom may change significantly, resulting in a change in Hubbard U parameter. The parameterization done in this study mainly focuses on neutral clusters. The Hubbard U parameter used in this study may not work well for charge system due to the reason given above. The charge dependence of Hubbard U parameter can only be accounted by using DFTB 3 (Gaus et al., 2012) which is outside the scope of this study. To avoid such complication which may occur in a charge system, this study will only focus on the search for ground state structure of neutral boron and BC clusters.

1.7 Structure of this Thesis

Chapter 1 provides an introduction to the research topic to be addressed by this thesis, including the background on the method, the research gap for global optimization search for GSS, the problem statement, motivation and objectives of this study. Chapter 2 gives a brief introduction to the theory and the approximation made in

DFTB. Chapter 3 provides the methodology undertaken to create SK files. Chapter 4 reviews the LESs reported for carbon, boron and mixed BC clusters at DFT level by previous publication. Chapter 5 reports and discusses the LESs obtained in this study at both DFTB and DFT level, and compares them against that of previous studies. The effectiveness and accuracy of the EMBH methodology employed in the thesis for predicting the GSS of the BC clusters' GSS are also assessed and concluded based on the results obtained in this chapter. Chapter 6 concludes the finding obtained in this study and provides a suggestion for possible future work based on the findings of this thesis.

CHAPTER 2 - THEORY

Quantum mechanics is the branch in physics that describes nature of matter and light at the scale of atoms and subatomic particles (Squires, n.d.). It can be used to derive most theories in classical physics (Oliveira, 2017). Different from classical physics, quantities in quantum mechanics such as energy, momentum and angular momentum are discrete instead of continuous. DFT is a quantum mechanical modeling methods used to study the properties of many-body system. As mentioned in subsection 1.2, DFT calculation is very time consuming especially when the system studied is large. Hence this study utilizes the semi-empirical method, DFTB, in addition to DFT to search for the GSS of boron and BC clusters.

Self-consistent charge DFTB (SCC-DFTB) is an approximation to DFT with charge self-consistency (Gaus et al., 2009). While being less accurate than DFT, SCC-DFTB is better suited to deal with large system (Gaus et al., 2009). SCC-DFTB originates from second-order Taylor expansion of the total DFT energy. A brief review about DFT will be provided before the derivation of SCC-DFTB. The global minimum search algorithm, Modified Basin Hopping (MBH), an integral part of the search strategy, that works hand-in-hand with DFTB and DFT to search for GSS for boron and BC clusters, will be also be discussed at the end of this chapter.

2.1 Density Functional Theory (DFT)

DFT mainly stems from Hohenberg-Kohn Theorems: (Hohenberg, Kohn, 1964)

1. *The external potential is a unique functional of electron density.* This means that electron density uniquely determines the external potential and hence the Hamiltonian operator.

2. For any positive definite trial density, ρ , such that $\int \rho(\mathbf{r})d\mathbf{r} = N$ then the electronic energy functional, $E[\rho]$, has energy greater than or equal to the ground state energy, E_0 :

$$E[\rho] \geq E_0 \quad (2.1)$$

The electronic energy functional contains three terms-the kinetic energy $K[\rho]$, the interaction with the external potential $V_{\text{ext}}[\rho]$, and the electron-electron interaction $E_{\text{ee}}[\rho]$:

$$E[\rho] = K[\rho] + E_{\text{ext}}[\rho] + E_{\text{ee}}[\rho] \quad (2.2)$$

To approximate these functionals, a fictitious system with N non-interacting electrons is introduced. Let ψ_i be the orbital of the i -th electron (thereafter ψ_i will be denoted as Kohn-Sham orbital). This system of non-interacting electrons has the same electron density as that of the true ground state

$$\rho(r) = \sum_{i=1}^N |\psi_i|^2 \quad (2.3)$$

Let R_α and Z_α refer to the position and the atomic number of α atom respectively.

The total number of atoms in the system is given by N_a . \mathbf{r}_i represents the position of electron i . In this system, the energy due to the external potential is given by

$$E_{\text{ext}}[\rho] = \sum_{i=1}^N \sum_{\alpha=1}^{N_a} \left\langle \psi_i \left| \frac{Z_\alpha}{|\mathbf{r}_i - \mathbf{R}_\alpha|} \right| \psi_i \right\rangle \quad (2.4)$$

The total kinetic energy of the non-interacting electrons is

$$K_s[\rho] = -\frac{1}{2} \sum_{i=1}^N \langle \psi_i | \nabla^2 | \psi_i \rangle \quad (2.5)$$

The classical Coulomb interaction, $E_H[\rho]$, is the major contributor to electron-electron interaction:

$$E_H[\rho] = \frac{1}{2} \sum_{i=1}^N \left\langle \psi_i \left| \frac{\rho(\mathbf{r})}{|\mathbf{r}_i - \mathbf{r}|} \right| \psi_i \right\rangle \quad (2.6)$$

The error made in using a non-interacting kinetic energy and treating the electron-electron interaction classically is corrected by the exchange-correlation (XC) energy:

$$E_{xc}[\rho] = (K[\rho] - K_s[\rho]) + (E_{ee}[\rho] - E_H[\rho]) \quad (2.7)$$

The energy functional can then be written in terms of the density built from non-interacting orbitals as

$$E[\rho] = K_s[\rho] + E_{ext}[\rho] + E_H[\rho] + E_{xc}[\rho] \quad (2.8)$$

Since electron density at the ground state is expected to produce minimum total electronic energy, E_0 , applying variational principle on energy functional, $E[\rho]$, subject to the constraint that the density contains the correct number of electrons, N , leads to the fundamental statement of density functional theory:

$$\delta\{E[\rho] - \mu(\int \rho(\mathbf{r})d\mathbf{r} - N)\} = 0 \quad (2.9)$$

The Lagrange multiplier of this constraint is the electronic chemical potential μ . (Leach, 2001b) Applying the variational principles leads to Kohn-Sham equation:

$$\left[-\frac{1}{2}\nabla^2 + V_{ext}(\mathbf{r}) + \int \frac{\rho(\mathbf{r}')}{|\mathbf{r}-\mathbf{r}'|}d\mathbf{r}' + V_{xc}(\mathbf{r})\right]\psi_i(\mathbf{r}) = \varepsilon_i\psi_i(\mathbf{r}) \quad (2.10)$$

where V_{xc} is the XC potential:

$$V_{xc}(\mathbf{r}) = \frac{\delta E_{xc}[\rho(\mathbf{r})]}{\delta \rho(\mathbf{r})} \quad (2.11)$$

$$V_{ext}(\mathbf{r}) = -\sum_{i=1}^N \sum_{\alpha=1}^{N_\alpha} \frac{Z_\alpha}{|\mathbf{r}_i - \mathbf{R}_\alpha|} \quad (2.12)$$

Since V_{xc} and the Coulomb interaction depends on ρ , the KS equations must be solved using a self-consistent procedure as depicted in Figure 2.1 so that ψ_i can be expressed as a linear combination of basis functions, ϕ_μ . This process starts with an initial electron density, ρ_0 , the Hamiltonian matrix, $H_{\mu\nu}$, is calculated: (Leach, 2001b)

$$H_{\mu\nu} = \int \phi_\mu(\mathbf{r})\left\{-\frac{\nabla^2}{2} + V_{ext}(\mathbf{r}) + \int \frac{\rho_0(\mathbf{r}')}{|\mathbf{r}-\mathbf{r}'|}d\mathbf{r}' + V_{xc}(\mathbf{r})\right\}\phi_\nu(\mathbf{r})d\mathbf{r} \quad (2.13)$$

Through solving the KS equation, a new electron density is obtained. Convergence is then checked. If the convergence criteria are not met, the new KS matrix is recalculated and the KS equation is solved again. This process is repeated until convergence is reached. The total energy is then calculated as:

$$E_{\text{tot}}[\rho] = K[\rho] + E_{\text{ext}}[\rho] + E_{\text{H}}[\rho] + E_{\text{xc}}[\rho] + E_{\text{nn}} \quad (2.14)$$

where E_{nn} is nucleus-nucleus repulsion.

The process to solve KS equation is similar to that of Roothaan-Hall equation. Leach (2001a) had provided a detailed description on how to solve Roothaan-Hall equation. He suggested that the simplest initial density matrix, P , is a null matrix (Leach, 2001a). This means the electron-electron interaction were temporarily ignored in the first loop (Leach, 2001a). This may lead to convergence problem which will be discussed later in subsection “SCF Convergence” in Chapter 3.

2.2 Self-Consistency Charge DFTB

Density Functional Tight Binding (DFTB) is a theory developed based on some approximations to DFT. The approximations made include (i) two-center approximation, (ii) the use of minimal basis functions in calculating the Hamiltonian and overlap matrix element, and (iii) a presumed pseudo-atomic electron density as starting density (Stock et al., 2012). The technical details of these approximations will be briefly reviewed in subsection 3.2. In DFTB calculation, the time-consuming evaluation of Hamiltonian and overlap matrix elements had been overcome by storing these matrix elements in the form of Slater-Koster (SK) file. This enables DFTB to perform a calculation more efficiently than DFT (Elstner et al., 2000). As a SK file describes the interactions between a pair of atoms, be it comprised of atom of the same species or otherwise, it is atom-specific in nature.

DFTB is an approximation to DFT. In self-consistent charge DFTB (SCC-DFTB), the electron density is solved self-consistently and energy due to charge fluctuation is taken into account. Consider a system of multiple atoms where bonds are not formed. The total electron density, ρ_0 , is the sum of the electronic density of

each individual atom. In a real system, bonds are formed between atoms leading to charge fluctuation. Hence, the electronic density of a real system, ρ , is written as the reference density ρ_0 plus a small charge fluctuation, $\delta\rho$,

$$\rho(\mathbf{r}) = \rho_0(\mathbf{r}) + \delta\rho(\mathbf{r}) \quad (2.15)$$

Expand the energy functional at ρ_0 to second order in a small charge fluctuation, $\delta\rho$: (Koskinen & Mäkinen, 2009)

$$\begin{aligned} E[\rho_0 + \delta\rho] &= \sum_{i=1}^N \langle \psi_i | -\frac{1}{2}\nabla^2 + V_{\text{ext}}(\mathbf{r}_i) + \int \frac{\rho_0'}{|\mathbf{r}-\mathbf{r}'|} d\mathbf{r}' + V_{\text{xc}}[\rho] | \psi_i \rangle \\ &+ \frac{1}{2} \iint \left(\frac{\delta^2 E_{\text{xc}}[\rho_0]}{\delta\rho\delta\rho_0} + \frac{1}{|\mathbf{r}-\mathbf{r}'|} \right) \delta\rho\delta\rho' dVdV' \\ &+ E_{\text{xc}}[\rho_0] + E_{\text{nn}} - \int V_{\text{xc}}[\rho_0]\rho_0 dV - \frac{1}{2} \iint \frac{\rho_0'}{|\mathbf{r}-\mathbf{r}'|} \rho_0 dVdV' \end{aligned} \quad (2.16)$$

The first line in equation (2.16) is the band-structure energy which depends only on $\rho_0(\mathbf{r})$. The second line is the energy due to charge fluctuations. The last line is called the repulsive energy as it is mainly made up of the ion-ion repulsion and electron-electron repulsion term. The repulsive potential is usually short range (Koskinen & Mäkinen, 2009).

Equation (2.16) can then be written as

$$E = E_{\text{BS}}[\rho_0] + E_{\text{coul}}[\delta\rho] + E_{\text{rep}}[\rho_0] \quad (2.17)$$

where

$$E_{\text{BS}}[\rho_0] = \sum_{i=1}^N \langle \psi_i | H^0 | \psi_i \rangle \quad (2.18)$$

$$E_{\text{coul}}[\delta\rho] = \frac{1}{2} \iint \left(\frac{\delta^2 E_{\text{xc}}[\rho(\mathbf{r})]}{\delta\rho(\mathbf{r}')\delta\rho(\mathbf{r})} \Big|_{\rho_0} + \frac{1}{|\mathbf{r}-\mathbf{r}'|} \right) \delta\rho(\mathbf{r})\delta\rho(\mathbf{r}') d\mathbf{r}d\mathbf{r}' \quad (2.19)$$

$$E_{\text{rep}}[\rho_0] = E_{\text{xc}}[\rho_0] + E_{\text{nn}} - \int V_{\text{xc}}[\rho_0(\mathbf{r})]\rho_0(\mathbf{r}) d\mathbf{r} - \frac{1}{2} \iint \frac{\rho_0'}{|\mathbf{r}-\mathbf{r}'|} \rho_0 dVdV' \quad (2.20)$$

H^0 is the Hamiltonian operator evaluated at ρ_0 . In SCC-DFTB, the KS equation must be solved for valence electrons iteratively to obtain the total energy of the system.

The Hamiltonian matrix elements take into account the charge fluctuation in each

atom. The repulsive energy will be read directly from the spline function in the SK file according to the bond length between the atom pairs. The following subsections will discuss the process of calculating band structure energy and energy from charge fluctuations.

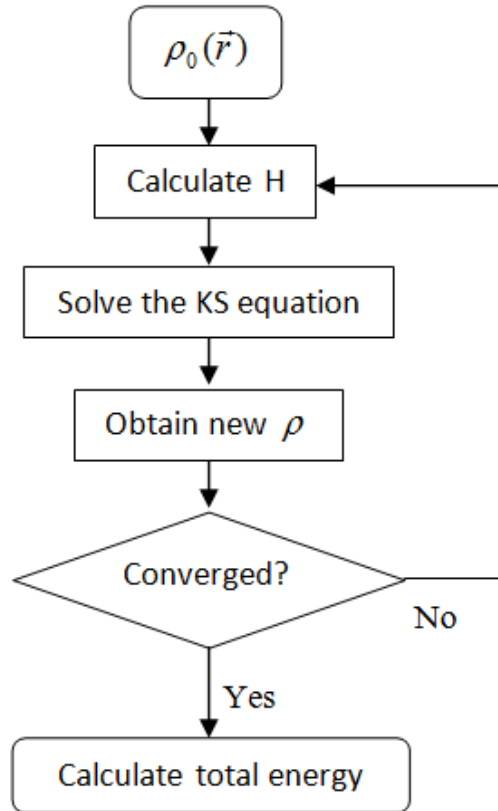


Figure 2.1 Flow chart of DFT calculation using Kohn-Sham method. Adopted from Ref. (Oliveira et al., 2009)

2.2.1 Band-Structure Energy

The band-structure energy is calculated using the following equation where n_i and ε_i are the occupation number and energy of KS orbital i respectively: (Oliveira et al., 2009)

$$E_{BS} = \sum_i n_i \varepsilon_i \quad (2.21)$$

$n_i = 2$ for doubly occupied orbital and 0 for virtual orbital.

2.2.2 Energy due to Charge Fluctuation

Let the density fluctuation be written as a superposition of the atomic-like contribution, $\delta\rho$:

$$\delta\rho = \sum_I \Delta q_I \delta\rho_I \quad (2.22)$$

$$\Delta q_I = q_I - q_I^0 \quad (2.23)$$

$$\int \delta\rho_I(\mathbf{r}) d\mathbf{r} = 1 \quad (2.24)$$

where q_I and q_I^0 are the Mulliken population and number of valence electrons for atom I , respectively. Equation (2.19) can then be written as

$$E_{\text{coul}}[\delta\rho] = \sum_{I,J} \left(\frac{1}{2} \Delta q_I \Delta q_J \gamma_{IJ} \right) \quad (2.25)$$

where

$$\gamma_{IJ} = \iint_{IJ} \left(\frac{\delta^2 E_{\text{xc}}}{\delta\rho_I \delta\rho_J} + \frac{1}{|\mathbf{r}_i - \mathbf{r}_j|} \right) \delta\rho_I \delta\rho_J d\mathbf{r}_I d\mathbf{r}_J \quad (2.26)$$

Let \mathbf{R}_I refers to the position of atom I . When $|\mathbf{R}_I - \mathbf{R}_J| \rightarrow \infty$, the exchange-correlation term will vanish. (Oliveira et al., 2009) Hence the energy due to charge fluctuation is given by (Oliveira et al., 2009)

$$E_{\text{coul}}[\delta\rho] = \frac{1}{2} \sum_{IJ} \frac{\Delta q_I \Delta q_J}{|\mathbf{R}_I - \mathbf{R}_J|} \quad (2.27)$$

To determine γ_{II} , consider an atom I with charge q_I . When atom I experiences a charge fluctuation Δq_I , the total energy E can be approximated by

$$E(\Delta q_I) \approx E_0 + \frac{\partial E}{\partial q_I} \Delta q_I + \frac{1}{2} \frac{\partial^2 E}{\partial q_I^2} (\Delta q_I)^2 \quad (2.28)$$

The second derivative $\frac{\partial^2 E}{\partial q_I^2}$ is identified as the Hubbard U parameter of atom I , i.e. U_I (Bodrog & Aradi, 2012). Hence the last term on the right hand side of equation (2.28) can be expressed as $\frac{1}{2} U_I \Delta q^2$. Comparing $\frac{1}{2} U_I (\Delta q_I)^2$ with the term $\frac{1}{2} \Delta q_I \Delta q_J \gamma_{IJ}$ at the right hand side of equation (2.25), γ_{II} can be identified as U_I when $I = J$. The

method to obtain the value of the Hubbard U parameter is discussed in subsection 3.3 as this chapter mainly discusses the theory of DFTB.

When the KS equation is solved iteratively, the charge fluctuation is reflected in the Hamiltonian term using the following equations: (Oliveira et al., 2009)

$$H_{\mu\nu} = H_{\mu\nu}^0 + H'_{\mu\nu} \quad (2.29)$$

where $H_{\mu\nu}^0$ is the Hamiltonian matrix element evaluated at ρ_0 and

$$H'_{\mu\nu} = \frac{S_{\mu\nu}}{2} \sum_I (\gamma_{\alpha I} + \gamma_{\beta I}) \Delta q_I, \mu \in \alpha, \nu \in \beta \quad (2.30)$$

2.2.3 Assumptions Made in SCC-DFTB

The assumptions made in SCC-DFTB are summarized below:

1. In DFTB, atomic orbitals (for valence shells only) are used as the minimal basis function to solve KS equation. The methods to obtain the atomic orbitals will be described in chapter 3.1. By inspecting equation (2.30), the impact of charge fluctuation on each orbital was taken into account in an average manner. In contrast, DFT used basis functions, such as 6-311+G(d) or aug-cc-pvdz, to obtain the KS orbital. In this manner, the distribution of electrons can be adjusted in each iteration by expressing the KS orbital as a linear combination of the basis function to minimize the total energy. Hence the distribution of electron can be described more accurately. In addition, the impact of charge fluctuation on each orbital can be taken into account more accurately compared to that of DFTB.
2. A precompiled electron density, ρ_0 , was used together with the atomic orbitals, ϕ_i , to calculate the Hamiltonian matrix element. To summarize the Hamiltonian matrix is calculated using the equation as follow: (Oliveira et al., 2009)

$$H_{\mu\nu}^0 = \begin{cases} \varepsilon_{\mu}^{\text{free}}, & \mu = \nu \\ \left(\phi_{\mu} \left| -\frac{1}{2}\nabla^2 + V_{\text{KS}}[\rho_0^{\alpha} + \rho_0^{\beta}] \right| \phi_{\nu} \right), & \mu \in \alpha, \nu \in \beta \\ 0, & \text{otherwise} \end{cases} \quad (2.31)$$

where $V_{\text{KS}}[\rho] = \sum_{i=\alpha,\beta} \frac{z_i}{|r-\mathbf{R}_i|} \int \frac{\rho(r')}{|r-r'|} d\mathbf{r}' + V_{\text{xc}}[\rho]$. The diagonal elements in the Hamiltonian matrix, $\varepsilon_{\mu}^{\text{free}}$, are chosen to be the energy of the atomic orbital μ in a free atom, which is known as the on-site energy. This choice ensures correct dissociation limit (Oliveira et al., 2009).

3. The two-center non-diagonal elements, as shown in equation (2.31), are calculated using two-center approximation and superposition of electron density ($\rho_0^{\alpha} + \rho_0^{\beta}$). Other elements in the Hamiltonian matrix equal to zero. In subsequent iterations, the impact of charge fluctuation on the Hamiltonian matrix element is taken into account as described in subsection 2.2.2.

2.3 Modified Basin Hopping

The research group from the National Central University of Taiwan led by Prof. Lai San Kiong has developed algorithms based on Basin Hopping (BH) and Genetic Algorithm (GA) that are specifically designed for locating the global minimum of cluster systems in their potential energy surface (Lai et al., 2002). These two algorithms were applied to search for the GSS of monovalent (Na, K, Rb, and Cs) and polyvalent (Pb) metals. Both algorithms yielded the same GSS (Lai et al., 2002). In 2015, the BH was modified to unbiasedly search for the GSS of the cluster made up of 60 carbon atoms, which are known to be the C_{60} fullerene structure (Lai, Yen, 2015). This effort has led to the development of a modified version to the original 2002 algorithm. The modified version is now known as Modified Basin Hopping (MBH). As MBH was mainly developed from BH, the discussion below will mainly

focus on BH instead of GA. The following paragraphs will discuss the features of BH followed by the modifications done to create MBH.

BH method was a very well-known algorithm first developed by Wales and Doye (Wales & Doye, 1997). The original BH is an optimization scheme for finding the global minimum in the potential energy surface (PES) of a system made up of Lenard-Jones particles. In Basin Hopping, a three-stage optimization method involves (1) generation of random clusters, (2) local minimization of the coordinates of the atoms, (3) acceptance or rejection of the new structure based on Metropolis criterion of standard Monte Carlo algorithms is adopted (Li & Scheraga, 1987). In the BH algorithm developed by Lai et al., random clusters are generated within a sphere with radius:

$$R_d = \left[1 + \left(\frac{3N_a}{4\pi\sqrt{2}} \right)^{\frac{1}{3}} \right] r_0 \quad (2.32)$$

where N_a and r_0 represent the number of atoms in the given composition and the nearest-neighbor distance. Angular move and random displacement (AMRD) is the operator used in BH to modify the structure of a cluster to generate new random cluster. Its operation is described as follow. The atom in a cluster, which is farthest from the origin, is located and its distance from the origin is then measured as r_{\max} . Suppose $V(i)$ is the potential of the i -th atom due to its interaction with all the other atoms. Let V_l and V_h be the lowest and highest potential energy after $V(i)$ is sorted. If $V_h > \nu V_l$, where ν is initially fixed at 0.36, the atom with energy V_h is moved to the surface of r_{\max} while other atoms are randomly displaced by δ where $0 < \delta < 1$. Otherwise, all atoms are randomly displaced by δ (Lai et al., 2002).

After the first stage perturbation of atoms as described above, a random cluster is produced. This cluster is then locally optimized so that the energy of the cluster is relaxed to the local minimum of the PES. This is the second stage of BH. In

the third stage, thermodynamics is taken into account in the process of accepting or rejecting a new optimized structure. Consider an optimized structure where its energy is E_{old} . To hop to another local minimum, this optimized structure is modified using AMRD to produce a new random structure. The new random structure is locally optimized where its energy is E_{new} . If $E_{\text{new}} < E_{\text{old}}$, the new structure is accepted. Otherwise, the probability distribution where there is a change in energy is given by

$$P(E_{\text{new}}|E_{\text{old}}) \sim e^{-(E_{\text{new}}-E_{\text{old}})/T} \quad (2.33)$$

Random number, λ , is generated and compared to $P(E_{\text{new}}|E_{\text{old}})$. If $\lambda < P(E_{\text{new}}|E_{\text{old}})$, the newly optimized structure is accepted. Otherwise, it is rejected. Doye, Wales, and Miller in (Doye et al., 1998) showed that the higher the temperature (T) in equation (2.33), the faster the system can explore different local minima. This method enables BH to overcome the energy barrier and trap in local minimum so that other local minima can be explored. In the basin-hopping algorithm developed by Lai's team, the temperature (T) is initially set at 0.8 K. The values of T and ν are subsequently adjusted by considering the acceptance rate of new structures (Lai et al., 2002).

MBH is modified from Lai's earlier BH method to strengthen the efficiency to find the LES for a cluster system. Details of the MBH algorithm can be found in ref. (Yen & Lai, 2015). Two modifications done were: (1) random clusters generated are confined in a sphere which radius is defined by the R_d^* , and (2) the introduction of cut-and-splice as a new operator to generate random clusters in addition to the existing AMRD. The radius of the sphere, R_d^* , is defined as

$$R_d^* = \alpha R_d = \alpha \left[1 + \left(\frac{3N_a}{4\pi\sqrt{2}} \right)^{\frac{1}{3}} \right] r_0 \quad (2.34)$$

where α a free parameter introduced for fine tuning the global search.